

Supporting Information

Interconnected Surface-Vacancy-Rich PtFe Nanowires for Efficient Oxygen Reduction†

Yanhong Shi^{a, b†}, Wei Yang^{b†}, Wenbin Gong^e, Xiaona Wang^b, Yurong Zhou^b, Xiaofan Shen^b, Yulong Wu^b, Jiangtao Di^{b, c, d}, Dongsong Zhang^{a*}, Qingwen Li^{b, c, d*}*

†These authors contributed equally to this work.

^a Department of Chemistry, College of Science, Shanghai University, Shanghai, 200438, China.

^b Key Laboratory of Multifunctional Nanomaterials and Smart Systems, Advanced Materials Division, Suzhou Institute of Nano-Tech and Nano-Bionics, Chinese Academy of Sciences, Suzhou 215123, China

^c School of Nano-Tech and Nano-Bionics, University of Science and Technology of China, Hefei 230026, China

^d Division of Nanomaterials, Suzhou Institute of Nano-Tech and Nano-Bionics, Chinese Academy of Sciences, Nanchang 330200, China

^e School of Physics and Energy, Xuzhou University of Technology, Xuzhou 221018, China

Correspondence and requests for materials should be addressed to *Jiangtao Di* (email: jtdi2009@sinano.ac.cn), *Dongsong zhang* (email: dszhang@shu.edu.cn) and *Qingwen Li* (email: qwli2007@sinano.ac.cn)

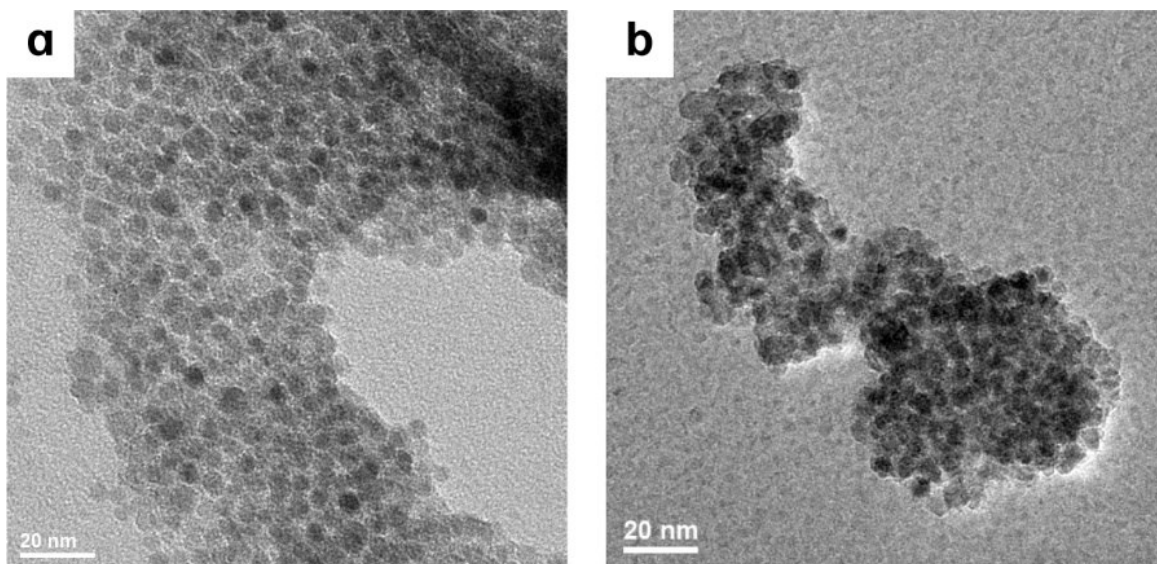


Figure S1. The TEM image of nanoparticles.

The Fe_3O_4 nanoparticles were spherical and exhibited suitable dispersion; they aggregated after being impregnated in the Na_2PtCl_6 solution, and still remained the nanoparticle state.

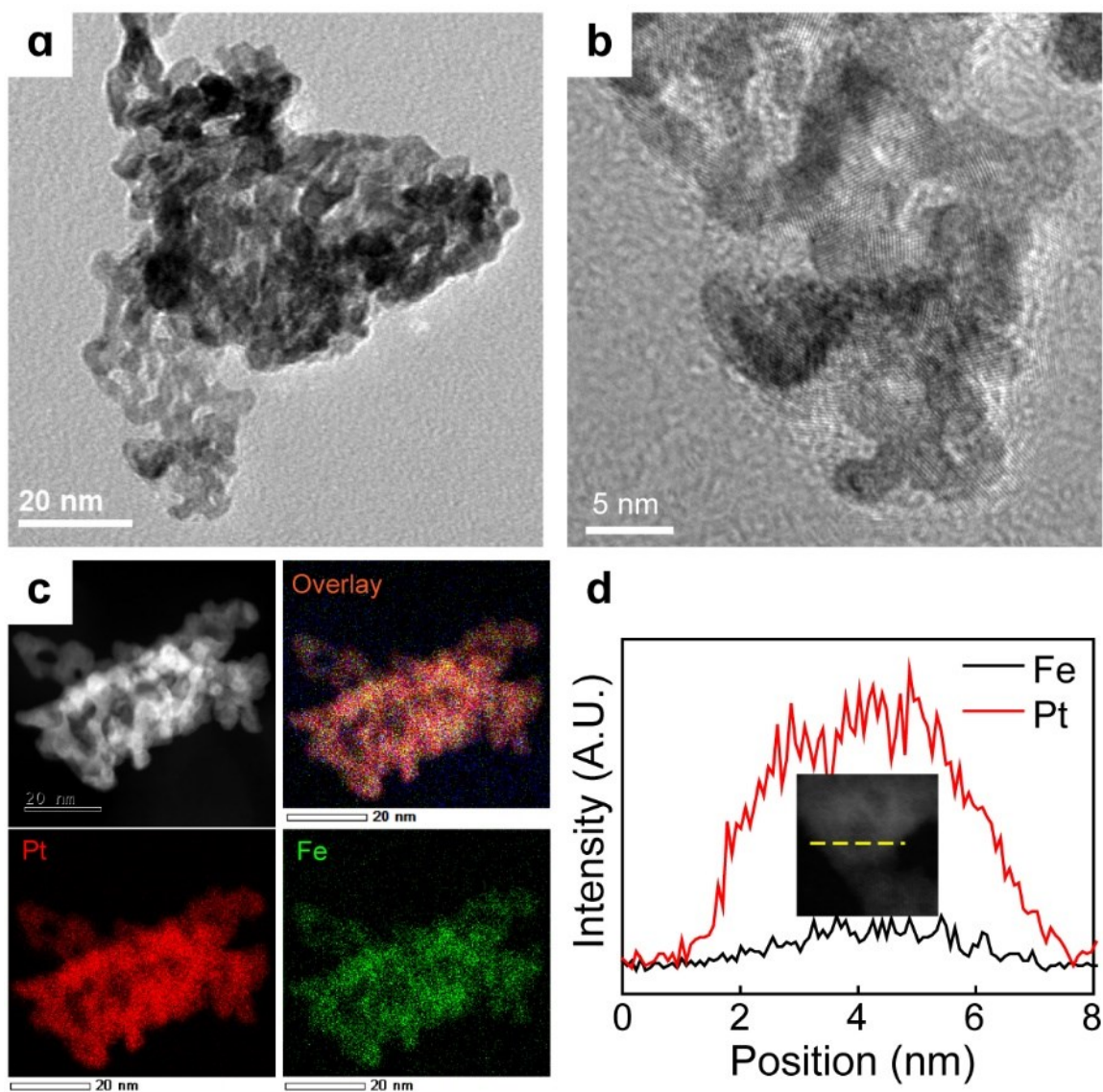


Figure S2 (a) TEM, (b) HR-TEM, (c) HAADF-STEM, and corresponding EDS mapping images, and (d) STEM-EDS line-scanning profile of PtFe/Pt NW.

The core-shell PtFe/Pt NNW annealed at 1000 °C with a uniform Pt-skin surface was also prepared. The morphology and structure of the as-prepared products were characterized by transmission electron microscopy (TEM) and spherical aberration-corrected electron microscopy. Due to the different diffusion rates of Pt and Fe atoms, a thick Pt-skin of the PtFe/Pt NNW was formed at 1000 °C, which hindered the formation of Fe vacancies.

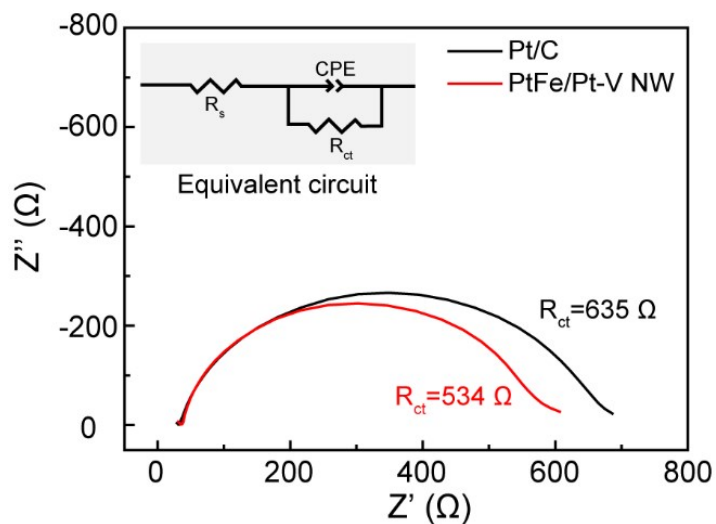


Figure S3 Nyquist plots of commercial Pt/C and PtFe/Pt-V NW at 0.9 V vs. RHE. The inset is the equivalent circuit diagram.

Figure S3 shows the Nyquist plots of commercial Pt/C and PtFe/Pt-V NW at 0.9 V vs. RHE. The charge transfer resistances, R_{ct} , of the Pt/C and the PtFe/Pt-V NW were 635 and 543 Ω , respectively, which suggests a faster electron transport in the PtFe/Pt-V NW.

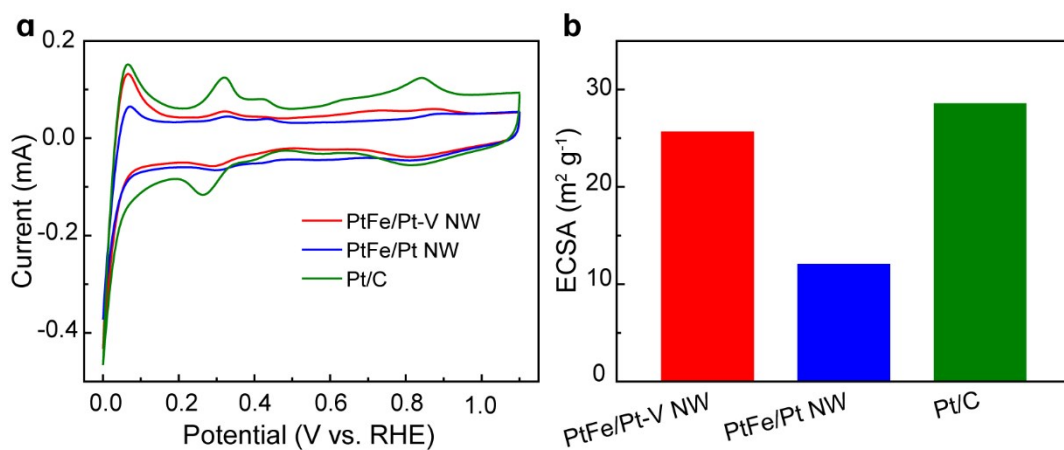


Figure S4 (a) CV curves and (b) corresponding ECSA calculated by H_{upd} of Pt/C, PtFe/Pt-V NW, and PtFe/Pt NW. CV was operated in Ar-saturated 0.1 M KOH at a sweep rate of 50 mV s^{-1} .

The electrochemically active surface area (ECSA) was measured by hydrogen underpotential deposition (H_{UPD}). The ECSA of PtFe/Pt-V NW ($25.6 \text{ m}^2 \text{ g}_{\text{Pt}}^{-1}$) was a little lower than Pt/C ($28.5 \text{ m}^2 \text{ g}_{\text{Pt}}^{-1}$), but was much higher than PtFe/Pt NW ($5.0 \text{ m}^2 \text{ g}_{\text{Pt}}^{-1}$).

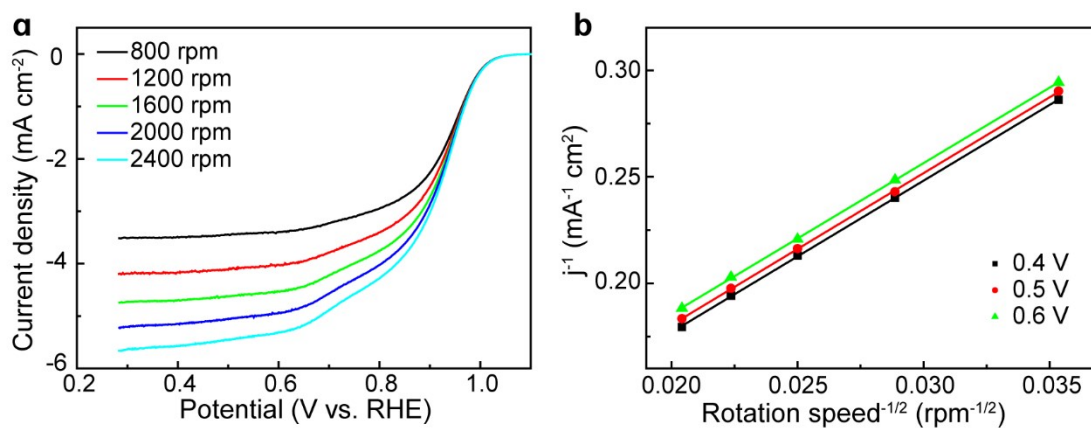


Figure S5 (a) LSV curves at different rotation speeds and (b) the corresponding K-L plots of PtFe/Pt NW. LSV was operated in O₂-saturated 0.1 M KOH at a sweep rate of 10 mV s⁻¹.

According to the Koutecky–Levich equation, the electron transfer number of the PtFe/Pt NW for ORR is calculated to be 4.0 ($n=4.0$), which indicates that the catalytic oxygen reduction reaction is approximately a 4-electron process in O₂-saturated 0.1 M KOH solution.

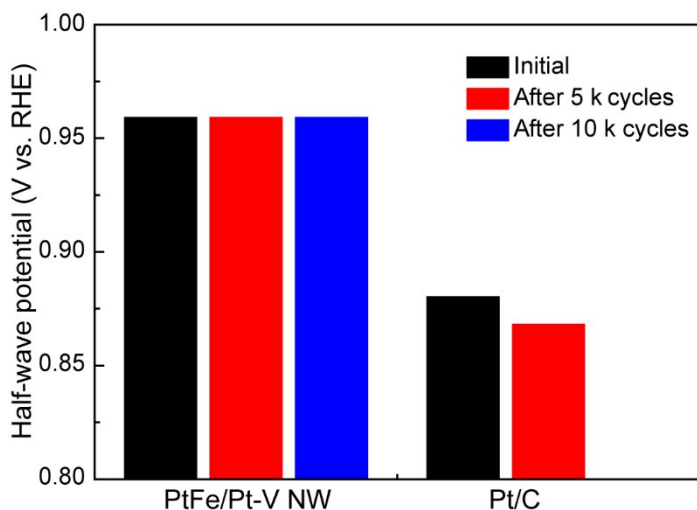


Figure S6 Half-wave potential changes of PtFe/Pt-V NW and Pt/C initially and after ADTs. ADTs were performed between 0.6 and 1.1 V (vs RHE) in O₂-saturated 0.1 M KOH at a sweep rate of 100 mV s⁻¹ and rotation speed of 1600 rpm.

The half-wave potential of PtFe/Pt-V NW showed no change after 10 k ADT cycles, but a significant decrease of 12 mV was observed for the Pt/C only after 5 k ADTs, which demonstrates that PtFe/Pt-V NW is much more stable than the commercial Pt/C catalyst.

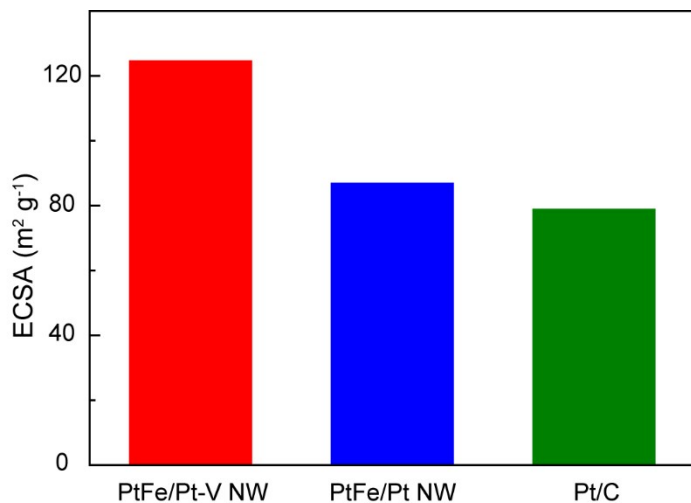


Figure S7 ECSA calculated by H_{upd} of Pt/C, PtFe/Pt-V NW, and PtFe/Pt NW in Ar-saturated 0.1 M HClO_4 .

The electrochemically active surface area (ECSA) measured by hydrogen underpotential deposition (H_{UPD}) for Pt/C, PtFe/Pt NW, and PtFe/Pt-V NW were $78.7 \text{ m}^2 \text{ g}^{-1}$, $86.8 \text{ m}^2 \text{ g}^{-1}$ and $124.5 \text{ m}^2 \text{ g}^{-1}$, respectively. This large ECSA of PtFe/Pt-V NW can be ascribed to the rich vacancies present on the Pt-skin surface, which can increase the catalytic active sites.

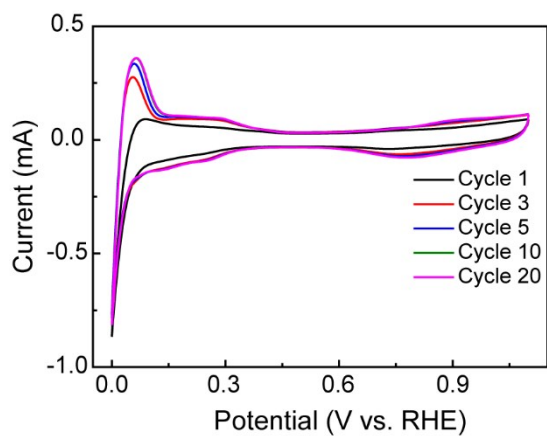


Figure S8 CVs of PtFe/Pt-V in 0.1 M HClO₄ solution.

The ECSA calculated by H_{upd} went up as the CV cycles increasing. During CV treatment, most of Fe atoms on the catalyst topmost and near-surface layers dissolved, form surface vacancy defects. Thus, it can be inferred that the large ECSA was ascribed to the rich vacancies present on the Pt-skin surface

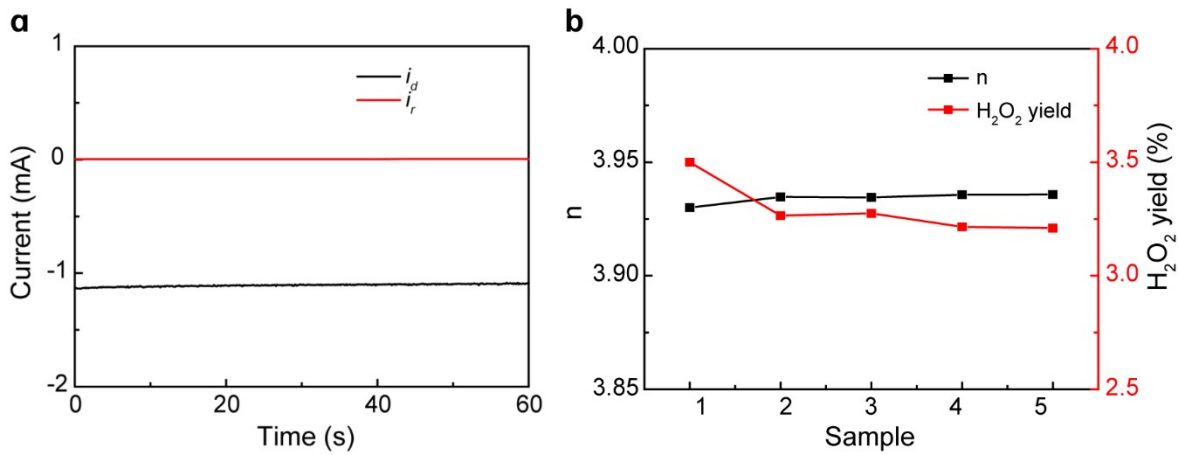


Figure S9 Figure S9. a. Amperometric i - t curves of PtFe/Pt-V NW. b. The n and H_2O_2 yield for ORR catalyzed by PtFe/Pt-V NW catalyst. The disk potential is 0.5 V vs. RHE, the ring potential is 1.5 vs. RHE.

The electron transfer number and H_2O_2 yield of the PtFe/Pt-V NW catalyst were calculated using a rotating ring-disk electrode by the following equation:

$$n = 4 \times \frac{i_d}{i_d + \frac{i_r}{N_c}}$$

$$H_2O_2\% = 200 \times \frac{\frac{i_r}{N_c}}{i_d + \frac{i_r}{N_c}}$$

Where n is the electron transfer number, i_d is the disk current, i_r is the ring current, and N_c is the collection efficiency ($n=0.32$). The i - t curves was tested at $E_d = 0.5$ V vs. RHE and $E_r = 1.5$ V vs. RHE for 2 minutes. The n and H_2O_2 yield were obtained as 3.93, 3.5%, respectively, which is consistent with the 4 electron-transfer process indicated by the Koutecky–Levich equation.

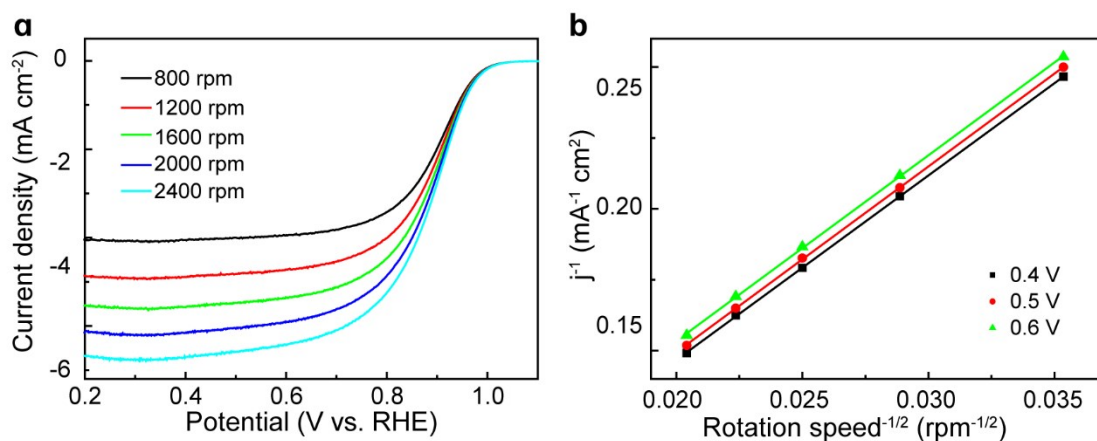


Figure S10 (a) LSV curves at different rotation speeds and (b) the corresponding K-L plots of PtFe/Pt NW. LSV was operated in O₂-saturated 0.1 M HClO₄ at a sweep rate of 10 mV s⁻¹.

According to the LSV curves for ORR at different rotation speeds and Koutecky–Levich equation, the electron transfer number of the PtFe/Pt NW for ORR is calculated to be 4.4 ($n=4.4$), which indicates that the catalytic oxygen reduction reaction is approximately a 4-electron process in O₂-saturated 0.1 M HClO₄ solution.

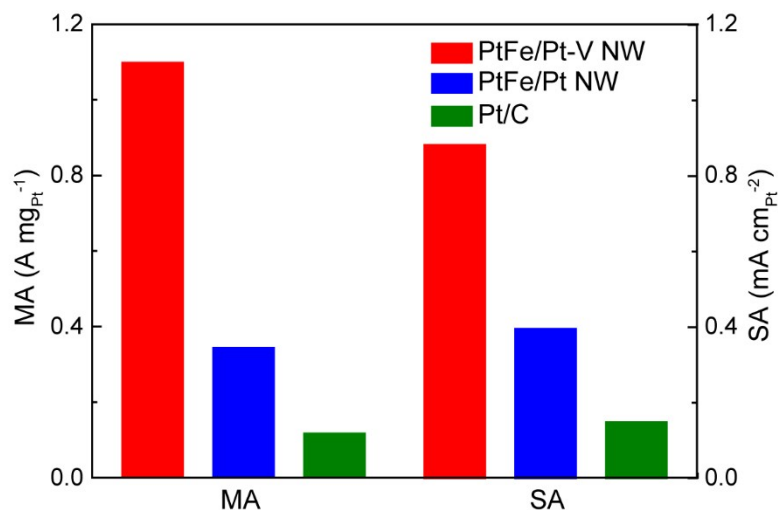


Figure S11 Mass and specific activities of Pt/C, PtFe/Pt-V NW, and PtFe/Pt NW at 0.9 V (vs RHE) in acidic medium.

The mass activities of Pt/C, PtFe/Pt-V NW, and PtFe/Pt NW were 0.11 A mg_{Pt}⁻¹, 1.10 A mg_{Pt}⁻¹, and 0.34 A mg_{Pt}⁻¹, respectively. The specific activities of Pt/C, PtFe/Pt-V NW, and PtFe/Pt NW were 0.15 mA cm_{Pt}⁻², 0.88 mA cm_{Pt}⁻², and 0.40 mA cm_{Pt}⁻² respectively. The PtFe/Pt-V NW displayed best mass and specific activities.

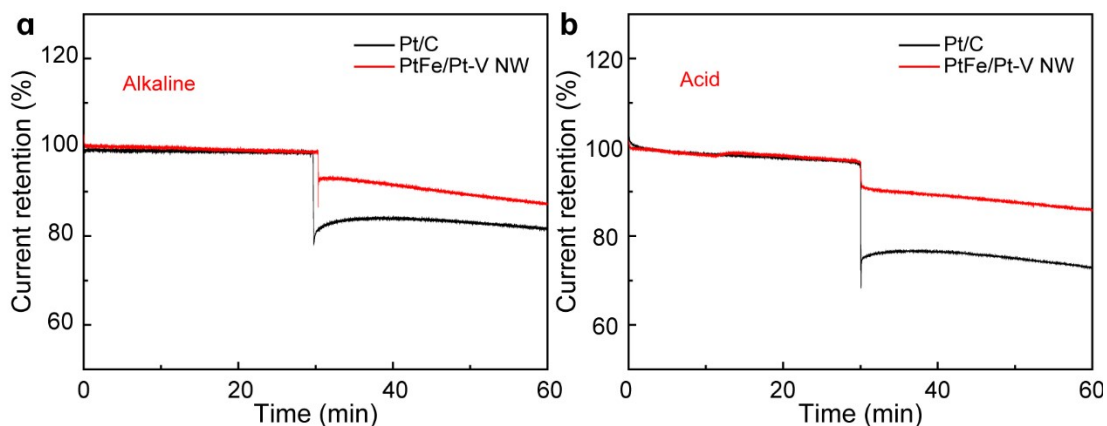


Figure S12 Methanol-tolerance performance of PtFe/Pt-V NW and 20 wt.% Pt/C. Current retention of Fe/Pt-V NW and 20 wt.% Pt/C before and after methanol injection in (a) 0.1 M KOH and (b) 0.1 HClO₄.

In alkaline solution, the current retention of PtFe/Pt-V NW kept almost 90%, whereas current density retention of the commercial 20 wt.% Pt/C decreased to ~80% after the methanol injection. In acid medium, the current retention of PtFe/Pt-V NW kept almost 95% after methanol injection, whereas current density retention of the commercial 20 wt.% Pt/C decreased to ~70%. These results demonstrated that PtFe/Pt-V NW had better methanol-tolerance performance than 20 wt.% Pt/C.

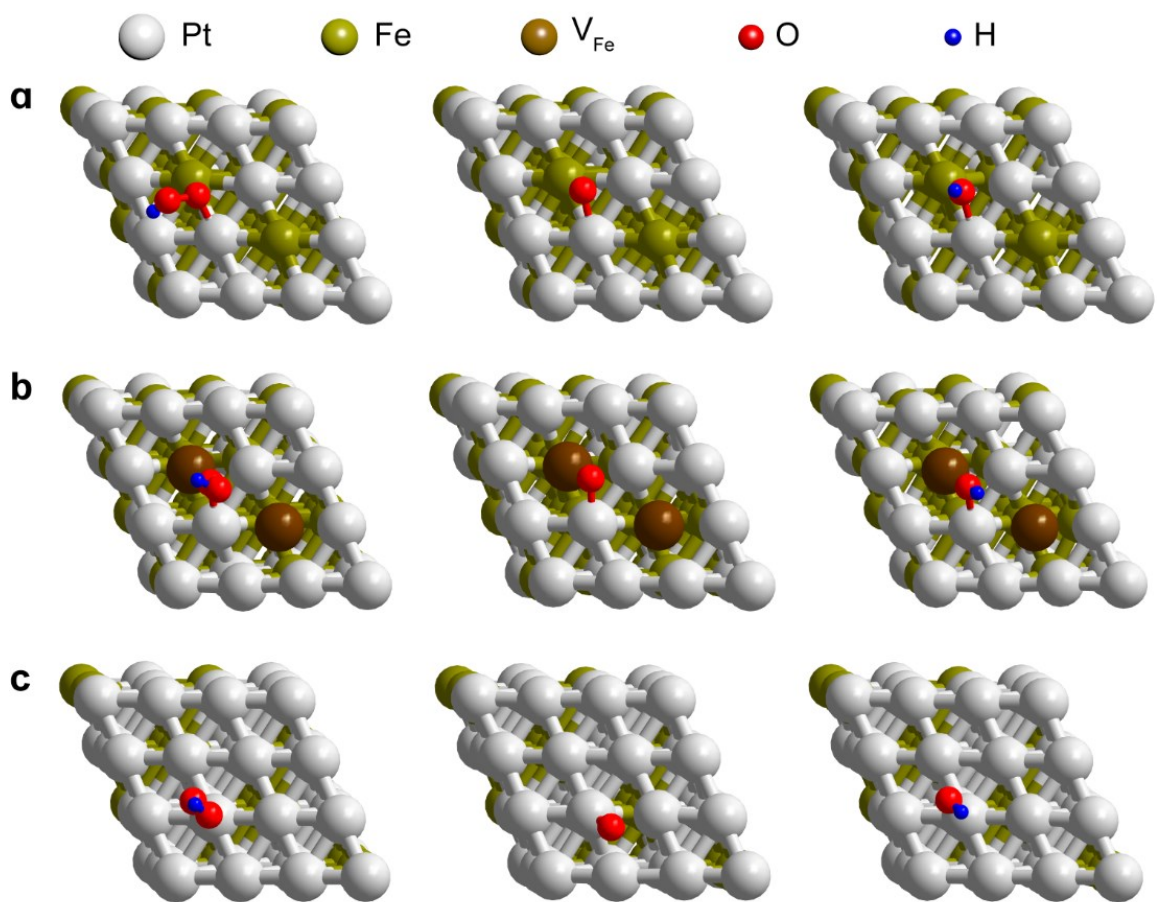


Figure S13. Adsorption structures of O-intermediates on (a) PtFe NW, (b) PtFe/Pt-V NW, and (c) PtFe/Pt NW (111) in vertical orientations: *OOH (left), *O (medium), and *OH (right).

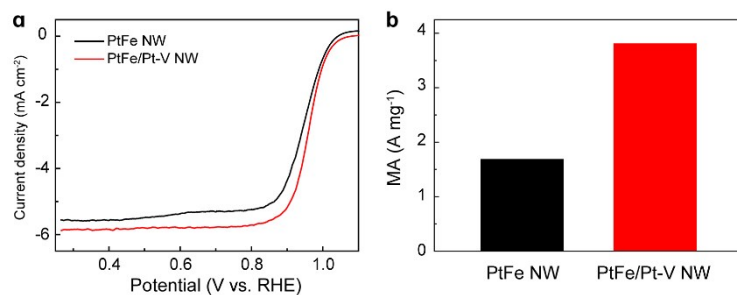


Figure. S14 ORR catalytic performance before and after electrochemical dealloying. (a) LSV curves of PtFe NW annealed at 900 °C. (b) MA comparison of PtFe NW before and after electrochemical dealloying.

Figure S14 compares the ORR catalytic performance of PtFe NW before and after electrochemical dealloying. The result demonstrated the vacancies on Pt-skin surface could boost the ORR activity of electrocatalysts, which was consisted with the DFT result.